SHUBNIKOV, A. V. (1951). *Symmetry and Antisymmetry of Finite Figures.* Moscow: Nauka.
SHUBNIKOV, A. V. & BELOV, N. V. (1964). *Colored Symmetry.* London: Pergamon Press.
SIROTIN, YU. I. & SHASKOL'SKAYA, M. P. (1982). *Fundamentals of Crystallophysics.* Moscow: Mir.
ZHELUDEV, I. S. (1964). *Kristallografiya,* **9**, 501-505.
ZHELUDEV, I. S. (1977). *At. Energy Rev.* **15**, N3, 461-492.
ZHELUDEV, I. S. (1983). *Symmetry and its Applications.* Moscow: Energoatomizdat.
ZHELUDEV, I. S. & VLOKH, O. G. (1983). *Proc. Indian Acad. Sci.* **92**, 421-427.

Acta Cryst. (1986). A**42**, 127-133

Experimental Determination of Triplet Phases and Enantiomorphs of Non-centrosymmetric Structures. I. Theoretical Considerations

BY K. HÜMMER AND H. BILLY

Institut für Angewandte Physik, Lehrstuhl für Kristallographie, Universität Erlangen-Nürnberg, Bismarckstrasse 6, *D*8520 *Erlangen, Federal Republic of Germany*

(*Received* 7 *January* 1985; *accepted* 11 *October* 1985)

Abstract

Information on the triplet phase sum Φ_Σ of the structure factor product $F(-\mathbf{h})F(\mathbf{h}-\mathbf{g})F(\mathbf{g})$ can be deduced from the rocking curve of a ψ-scan experiment scanning through a three-beam position. For non-centrosymmetric structures, four typical profiles can be observed. For $\Phi_\Sigma = 0, 180°$, asymmetric profiles result, whereas a nearly symmetrical decrease or increase of the two-beam intensity appears for $\Phi_\Sigma = \pm 90°$. In a first approximation this behaviour can be explained by the interference between the directly diffracted wave of **h** and the 'Renninger *Umweg*' wave of **g** and **h**−**g**. Their phase relationship and the amplitudes are governed by a spatial resonance term, which causes a phase shift of 180° and a continuously turning on and off of the *Umweg* wave amplitude scanning through the three-beam position. This interference can be displayed by a phase-vector diagram which outlines the main features of the ψ-scan profiles. The semi-quantitative results are confirmed by calculation based on the dynamical theory. The distinction between $\Phi_\Sigma = \pm 90°$ allows the experimental determination of enantiomorphs.

1. Introduction

It has been suggested for a long time that multiple-beam X-ray diffraction can be applied to determine the phase relationship of the waves involved. In a three-beam diffraction case three reciprocal-lattice points (r.l.p.) *O*, *H*, *G* simultaneously lie on or close to the Ewald sphere. Then, three strong wave fields are propagated in the crystal owing to the reciprocal-lattice vectors (r.l.v.) **O**, **h**, **g** with the propagating vectors $\mathbf{K}(\mathbf{n}) = \mathbf{K}(\mathbf{O}) + \mathbf{n}$, $\mathbf{n} = \mathbf{O}$, **h**, **g**, according to Bragg's law. From a more or less kinematical point of view, the amplitude of the total wave field propagated in the direction $\mathbf{K}(\mathbf{h})$ results from the interference between the 'direct' wave diffracted at the lattice plane (**h**) and the detour excited wave ('Renninger *Umweg*' wave) diffracted at the lattice planes (**g**) and (**h**−**g**). This depends on the phase difference and on the amplitudes of both waves given by their structure factors $F(\mathbf{h})$, $F(\mathbf{g})$ and $F(\mathbf{h}-\mathbf{g})$, respectively. Therefore, the diffracted intensity in the three-beam case bears information on the phase difference (Lipscomb, 1949):

$$\Phi_\Sigma = [\varphi(\mathbf{g}) + \varphi(\mathbf{h}-\mathbf{g})] - \varphi(\mathbf{h})$$
$$= \varphi(-\mathbf{h}) + \varphi(\mathbf{g}) + \varphi(\mathbf{h}-\mathbf{g}),$$

which represents a structure-invariant triplet phase relationship. The influence of this interference on the two-beam intensity can be measured by a Ψ-scan experiment monitoring the integrated intensity $I(\mathbf{h})$ while the crystal is rotated about the direction **h** and scanned through a three-beam position. The resultant Ψ-scan profiles must depend on the triplet phase Φ_Σ. They can be explained by the continuously turning on and off of the amplitude of the *Umweg* wave and an additional phase shift $\Delta(\Psi)$ by 180° when the r.l.p. *G* passes through the Ewald sphere (Hümmer & Billy, 1982).* If it is borne in mind that Bragg diffraction is a spatial resonance phenomenon (Ewald, 1917), the behaviour of the *Umweg* wave is nothing but the behaviour of every resonance phenomenon passing through the resonance.

* In the cited paper there is an error. $\Psi < 0$ and $\Psi > 0$ correctly mean that the third r.l.p. *G* lies inside or outside the Ewald sphere respectively, *i.e.* all the Ψ-scan profiles drawn in the paper refer to an in-out rotation sense.

0108-7673/86/020127-07$01.50

Starting from simplified fundamental equations of the dynamical theory of X-ray diffraction and applying a perturbational approach, we derive in this paper expressions for the amplitude and the intensity of the wave fields which proves the validity of our interpretation. The results can be outlined by a simple phase-vector diagram describing the interference between the directly diffracted and the *Umweg* wave. The phase-vector diagram immediately displays the general features of the Ψ-scan rocking curves for different triplet phases Φ_Σ even in the case of non-centrosymmetric crystal structures.

The experimental determination of structure-invariant triplet phases also allows the fixing of the absolute configuration because the triplet phases of enantiomorphs differ in their signs and the Ψ-scan profiles for $\Phi_\Sigma = \pm 90°$ are clearly distinguishable.

2. Spatial resonance

In order to calculate the amplitudes of the X-ray wave fields in an ideal crystal, one has to solve Maxwell's equations in a medium with a periodic complex dielectric susceptibility χ. This leads to the wave equation for the vector **D** of dielectric displacement

$$\mathrm{d}^2\mathbf{D}/\mathrm{d}r^2 + 4\pi^2 k_0^2 \mathbf{D} = -\mathrm{curl}\ \mathrm{curl}\ \mathbf{P} \qquad (1)$$

$$4\pi\mathbf{P} = \chi(\mathbf{r})\mathbf{D}; \qquad |\mathbf{k}_0| = \lambda_0^{-1},$$

which may be solved by the following relationships taking account of all the waves consistent with Bragg's law:

$$\mathbf{K}(\mathbf{h}) = \mathbf{K}(\mathbf{O}) + \mathbf{h}, \qquad (2)$$

$$\mathbf{P} = \exp(2\pi i\nu t) \sum_{\mathbf{h}} \mathbf{P}(\mathbf{h}) \exp[-2\pi i \mathbf{K}(\mathbf{h}) \cdot \mathbf{r}] \qquad (3)$$

$$\mathbf{D} = \exp(2\pi i\nu t) \sum_{\mathbf{h}} \mathbf{D}(\mathbf{h}) \exp[-2\pi i \mathbf{K}(\mathbf{h}) \cdot \mathbf{r}] \qquad (4)$$

$$\chi(\mathbf{r}) = \sum_{\mathbf{h}} \chi(\mathbf{h}) \exp(-2\pi i\nu \mathbf{h} \cdot \mathbf{r}); \ \chi(\mathbf{h}) = -\Gamma F(\mathbf{h}). \qquad (5)$$

P is the vector of dielectric polarization, $\mathbf{k}_0$ and $\mathbf{K}(\mathbf{h})$ are the wave vectors in the vacuum and inside the crystal, ν is the X-ray frequency, $\Gamma = r_e\lambda^2/\pi V_{EZ}$ (r_e: classical electron radius; V_{EZ}: volume of the elementary cell) is a small number of the order of 10^{-7} and $F(\mathbf{h})$ is the structure factor.

The solutions of (1) are the fundamental equations of the dynamical theory:

$$\mathbf{D}(\mathbf{h}) = -\{K(\mathbf{h})^2/[K(\mathbf{h})^2 - K^2]\}\Gamma \sum_{g \neq h} F(\mathbf{h}-\mathbf{g})\mathbf{D}_h(\mathbf{g});$$

$$|\mathbf{K}| = |k_0|[1 - \tfrac{1}{2}\Gamma F(\mathbf{O})]. \qquad (6)$$

$\mathbf{D}_h(\mathbf{g})$ is the projection of $\mathbf{D}(\mathbf{g})$ on $\mathbf{D}(\mathbf{h})$; $|K|$ is the radius of the Ewald sphere about the Lorentz point and it represents the wave vector in the one-beam case, *i.e.* only the r.l.p. *O* lies on the sphere.

In his work on crystal optics of X-rays Ewald (1965) pointed out that the dipole wave given by **P** travelling through the lattice is the 'driving force' for the displacement field strength $\mathbf{D}(\mathbf{h})$ of a certain wave vector $\mathbf{K}(\mathbf{h})$. The resonance term $[K(\mathbf{h}^2) - K^2]^{-1}$ may be regarded as the efficiency of the crystal for converting a given amplitude of polarization **P** into the field amplitude $\mathbf{D}(\mathbf{h})$. If Bragg's diffraction condition $K^2(\mathbf{h}) = K^2$ is fulfilled this efficiency will be optimum. The amplitudes $\mathbf{D}(\mathbf{h})$ of waves, the corresponding r.l.p.'s of which lie respectively outside $[K(\mathbf{h})^2 > K^2]$ or inside $[K(\mathbf{h})^2 < K^2]$ the Ewald sphere, undergo a change of their signs when crossing the sphere, *i.e.* there is a phase shift of 180° going through the resonance $K^2(\mathbf{h}) = K^2$ (Ewald, 1917) and the amplitude is turned on and off continuously. Thus, Bragg diffraction is a spatial resonance phenomenon, the diffraction is optimum when the spatial periodicity of the incoming wave matches the spatial periodicity of the lattice planes.

3. Interference near a three-beam setting

In the following, we calculate the amplitude of the wave fields near a three-beam case by a perturbational approach, which is common in electron diffraction dynamical theory and is often referred to as 'Bethe potentials' (Bethe, 1928). In their papers, Juretschke (1982*a*, *b*, 1984) and Høier & Marthinsen (1983) also used this formalism.

For simplicity we neglect the coupling terms due to different directions of polarization of the wave fields in the fundamental equations for a three-beam case and so we are left with the following system of equations for one direction of polarization only (Laue, 1960):

$$\begin{bmatrix} \dfrac{K(\mathbf{O})^2 - K^2}{K(\mathbf{O})^2} & \alpha_h^0 F(-\mathbf{h}) & \alpha_g^0 F(-\mathbf{g}) \\ \alpha_h^0 F(\mathbf{h}) & \dfrac{K(\mathbf{h})^2 - K^2}{K(\mathbf{h})^2} & \alpha_g^h F(\mathbf{h}-\mathbf{g}) \\ \alpha_g^0 F(\mathbf{g}) & \alpha_g^h F(\mathbf{g}-\mathbf{h}) & \dfrac{K(\mathbf{g})^2 - K^2}{K(\mathbf{g})^2} \end{bmatrix} \begin{bmatrix} D(\mathbf{O}) \\ D(\mathbf{h}) \\ D(\mathbf{g}) \end{bmatrix} = 0. \qquad (7)$$

α are geometrical coupling factors times Γ.

$D(\mathbf{g})$ may then be expressed in terms of the amplitudes of the wave fields $D(\mathbf{O})$ and $D(\mathbf{h})$ by the third line of (7):

$$D(\mathbf{g}) = -\{K(\mathbf{g})^2/[K(\mathbf{g})^2 - K^2]\} \times [\alpha_g^0 F(\mathbf{g}) D(\mathbf{O}) + \alpha_g^h F(\mathbf{g}-\mathbf{h}) D(\mathbf{h})]. \qquad (8)$$

Upon insertion of (8) in (7) the three-beam case can be reduced to give a modified two-beam case with an effective structure factor $F_{\mathrm{eff}}^{\pm}$.

$$\begin{bmatrix} -R(\mathbf{O})^{-1} + R(\mathbf{g})\alpha_g^{02}F^2(\mathbf{g}) & F_{\mathrm{eff}}^{-} \\ F_{\mathrm{eff}}^{+} & -R(\mathbf{h})^{-1} + R(\mathbf{g})\alpha_g^{h2}F^2(\mathbf{h}-\mathbf{g}) \end{bmatrix} \begin{bmatrix} D(\mathbf{O}) \\ D(\mathbf{h}) \end{bmatrix} = 0, \qquad (9)$$

where we use the following abbreviations:

$$R(\mathbf{n}) = \{K(\mathbf{n})^2/[K^2 - K(\mathbf{n})^2]\}; \qquad n = \mathbf{O}, \mathbf{g}, \mathbf{h}$$

$$F_{\text{eff}}^{\pm} = \alpha_h^0 F(\pm\mathbf{h}) + R(\mathbf{g})\alpha_g^0 \alpha_g^h F(\pm\mathbf{g}) F(\pm\mathbf{h} \mp \mathbf{g}). \quad (10)$$

Then, the ratio $D(\mathbf{h})/D(\mathbf{O})$ is given by

$$D(\mathbf{h})/D(\mathbf{O}) = R(\mathbf{h}) F_{\text{eff}}^{+}/N = [R(\mathbf{h})/N][D_2(\mathbf{h}) + D_u(\mathbf{h}, \mathbf{g})] \quad (11)$$

with

$$D_2(\mathbf{h}) = \alpha_h^0 F(\mathbf{h}); \; D_u(\mathbf{h}, \mathbf{g}) = R(\mathbf{g})\alpha_g^0 \alpha_g^h F(\mathbf{g}) F(\mathbf{h} - \mathbf{g});$$
$$N = 1 - \alpha_g^{h2} F^2(\mathbf{h} - \mathbf{g}) R(\mathbf{g}) R(\mathbf{h}).$$

This result confirms the basic idea of Lipscomb (1949). The amplitude of the wave field propagated in the $\mathbf{K}(\mathbf{h})$ direction is given by the superposition of the direct wave $D_2(\mathbf{h})$ (the index 2 indicates the two-beam amplitude) and the *Umweg* wave $D_u(\mathbf{h}, \mathbf{g})$. The phase difference of the waves is a triplet phase relationship. This can be clearly seen by rewriting (11):

$$D(\mathbf{h})/D(\mathbf{O}) = [R(\mathbf{h})/N] F(\mathbf{h}) \alpha_h^0 \{1 + [A/F^2(\mathbf{h})] \times R(\mathbf{g}) F(-\mathbf{h}) F(\mathbf{g}) F(\mathbf{h} - \mathbf{g})\} \quad (12)$$

with

$$A = \alpha_g^0 \alpha_g^h / \alpha_h^0.$$

The resonance term $R(\mathbf{g})$ governs the amplitude and the resonance phase shift of the *Umweg* wave. If the r.l.p. G is inside the Ewald sphere then $|K(\mathbf{g})| < |K|$ and $R(\mathbf{g}) > 0$. If it is outside then $|K(\mathbf{g})| > |K|$ and $R(\mathbf{g}) < 0$. That means that the amplitude of the *Umweg* wave changes its sign, *i.e.* there is a resonance phase shift $\Delta(\Psi)$ of 180° depending on the scanning angle Ψ in addition to the constant triplet phase. Therefore, the total phase difference $\Phi(\Psi)$ between the direct wave and the *Umweg* wave depends on Ψ and is given by

$$\Phi(\Psi) = \Phi_\Sigma + \Delta(\Psi). \quad (13)$$

The amplitude D_u is highest near the three-beam position for $|K(\mathbf{g})| \simeq |\mathbf{K}|$. By scanning through the three-beam resonance the amplitude of the *Umweg* wave is turned on and off continuously.

In a first-order approximation the interference between the direct and the *Umweg* wave can now be outlined by a simple phase-vector diagram. 'First-order approximation' means that the denominator N may be taken as a constant ($N \simeq 1$). It is equivalent to the range of validity for the first-order solution given by Juretschke (1984). In this range the main effect of the three-beam coupling is described by the effective structure factor F_{eff} which contains the phase-dependent terms. The range of validity for the first-order solution depends on the moduli of the structure factors involved in the three-beam case [Juretschke (1984), where ξ_L is equivalent to $1/R(\mathbf{g})$ in this work].

For the behaviour of the amplitude of the *Umweg* wave the resonance term $R(\mathbf{g})$ plays the important role. $R(\mathbf{g})$ is complex, bearing in mind that because of the absorption the wave vectors must be taken as complex numbers.

$$R(\mathbf{g}) = [K'(\mathbf{g}) - iK''(\mathbf{g})]^2/\{(K' - iK'')^2 - [K'(\mathbf{g}) - iK''(\mathbf{g})]^2\} = K'(\mathbf{g})^2/[K'^2 - K'(\mathbf{g})^2 + i\hat{K}^2] \quad (14)$$

with

$$\hat{K}^2 = 2K'K'(\mathbf{g})[K'K''(\mathbf{g}) - K'(\mathbf{g})K'']/K'(\mathbf{g})^2.$$

This is a Lorentzian-type function where we have neglected the quadratic terms of the imaginary parts which are some orders of magnitude smaller than the real parts. The decomposition into the modulus $R_g(\Psi)$ and the phase $\Delta(\Psi)$ leads to

$$R(\mathbf{g}) = R_g(\Psi) \exp[i\Delta(\Psi)]. \quad (15)$$

Fig. 1(*a*) shows typical resonance curves for both the amplitude $R_g(\Psi)$ and the phase $\Delta(\Psi)$. In the complex plane the terminal of the vector representing $R(\mathbf{g})$ traces out a circle by scanning Ψ through the three-beam position. So does the vector representing $D_u(\mathbf{h}, \mathbf{g})$ (*cf.* Fig. 1*b*).

The phase-vector diagram for the interference of the direct wave $D_2(\mathbf{h})$ and the *Umweg* wave $D_u(\mathbf{h}, \mathbf{g})$

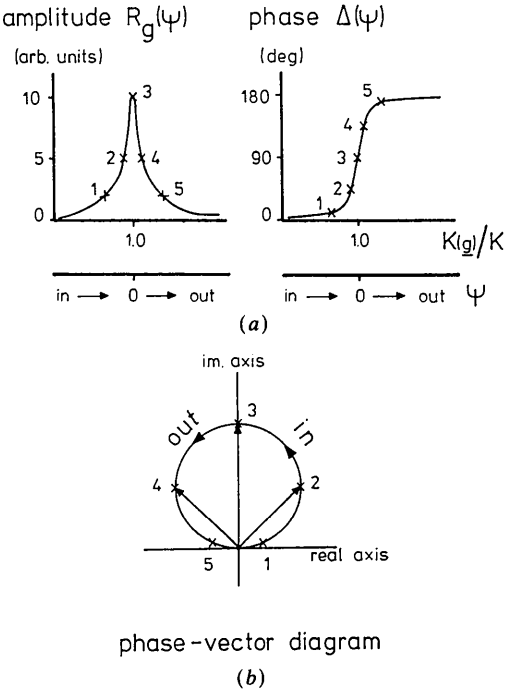

Fig. 1. Schematic drawing of the behaviour of the *Umweg* wave; (*a*) amplitude and phase *versus* scanning angle ψ; (*b*) the corresponding phase-vector diagram.

in a Ψ-scan experiment can now be constructed (Fig. 2). The real axis defines the reference angle zero for the *Umweg* wave, because only the phase difference of $D_2(\mathbf{h})$ and $D_u(\mathbf{h},\mathbf{g})$ is important and so we arbitrarily assign to $D_2(\mathbf{h})$ a phase of zero; *i.e.* $D_2(\mathbf{h})$ is given by a constant vector on the real axis. Then, the vector $D_u(\mathbf{h},\mathbf{g})$, tracing out a circle, is added. By rotation of its circle with respect to the real axis the constant triplet phase Φ_Σ is taken into account. The sum of these vectors gives the resultant wave amplitude $D(\mathbf{h})$ for the three-beam interference. The dashed circle about the origin with radius $D_2(\mathbf{h})$ is a subsidiary line. If the vector terminal of $D(\mathbf{h})$ lies outside then the resultant amplitude is larger, if it is inside, $D(\mathbf{h})$ is smaller than the amplitude $D_2(\mathbf{h})$ established by the two-beam diffraction, *i.e.* the three-beam intensity is increased or decreased with respect to the two-beam intensity $I^{(2)}(\mathbf{h})$. The general features of the Ψ-scan profiles for different triplet phases Φ_Σ can immediately be deduced from this phase-vector diagram.

The fundamental characteristics of the Ψ-scan profiles can also be easily calculated by means of (11) except for a range very close to the three-beam setting. But for $|\Psi|>2''$ $N\simeq 1$ and therefore the following relations hold:

$$I_h(\Psi)\sim|D(\mathbf{h})|^2=D(\mathbf{h})D^*(\mathbf{h})$$

$$I_h(\Psi)\sim[\alpha_h^0F(\mathbf{h})+R_g(\Psi)\times\exp i\Delta(\Psi)\alpha_g^0\alpha_g^hF(\mathbf{g})F(\mathbf{h}-\mathbf{g})]\times\text{complex conjugate}$$

$$I_h(\Psi)\sim\alpha_h^{02}|F(\mathbf{h})|^2+R_g^2(\Psi)\alpha_g^{02}\alpha_g^{h2}|F(\mathbf{g})|^2|F(\mathbf{h}-\mathbf{g})|^2+2CR_g(\Psi)\cos[\Phi_\Sigma+\Delta(\Psi)] \qquad (16)$$

with

$$C=\alpha_h^0\alpha_g^0\alpha_g^h|F(-\mathbf{h})||F(\mathbf{g})||F(\mathbf{h}-\mathbf{g})|.$$

Equation (16) also shows clearly the interference between the direct wave and the *Umweg* wave. It should be stressed that the interference term, the third term of (16), contains not only the triplet phase Φ_Σ but the interference is governed by the total phase difference $\Phi_\Sigma+\Delta(\Psi)$ [see (13)]. Since the intensity does not simply depend on cos Φ_Σ, different Ψ-scan profiles must result for $\Phi_\Sigma=\pm90°$. This difference cannot be deduced from the dispersion surfaces because they depend only on cos Φ_Σ (Ewald & Héno, 1968).

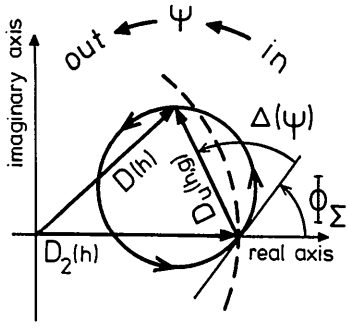

Fig. 2. Phase-vector diagram of the interference between the direct diffracted wave $D_2(\mathbf{h})$ and the *Umweg* wave $D_u(\mathbf{h},\mathbf{g})$.

4. Ψ-scan profiles for non-centrosymmetric structures

In the following it will be shown that the general features of the typical Ψ-scan profiles for triplet phases $\Phi_\Sigma=0$, ±90, 180° can be deduced from the phase-vector diagram (§ 4*a*). The results of this semi-quantitative discussion will be confirmed by Ψ-scan profiles calculated on the basis of the exact dynamical theory for a three-beam case (§ 4*b*).

For all the profiles the rotation sense of the Ψ scan is chosen so that the third r.l.p. G crosses the Ewald sphere from inside ($\Psi<0$) to outside ($\Psi>0$) (in-out case). For an out-in case the profiles must be read from right to left (Chang, 1982).

(*a*) *Semi-quantitative discussion*

Let us begin with $\Phi_\Sigma=0°$. At the onset of the three-beam diffraction the interfering waves are essentially in phase and scanning towards the exact three-beam setting, the *Umweg* wave amplitude growth. So is the intensity. Close to and scanning through the three-beam position, the total phase difference is shifted from 0 to 180° caused by the resonance phase shift $\Delta(\Psi)$ (*cf.* Fig. 1*a*). Then, the waves are out of phase [$\Phi(\Psi)=0+180°$] and the intensity drops below the two-beam level $I^{(2)}(\mathbf{h})$. When the r.l.p. G leaves the Ewald sphere the *Umweg* amplitude decreases to zero (Fig. 1*a*), *i.e.* the intensity approaches again the two-beam level. This typical asymmetry of the Ψ-scan profile can be immediately seen from the corresponding phase-vector diagram (Fig. 3*a*). Equation (16) leads to the same type of asymmetry taking into account the resonance phase shift of 180°. For simplicity one may neglect the second term of (16); it is at least one order of magnitude smaller in the range considered ($|\Psi|>2''$).

This type of asymmetry is reversed for a triplet phase $\Phi_\Sigma=180°$, because scanning through the three-beam position (in-out) the interfering waves are at first out of phase [$\Phi(\Psi)=180+0°$] and then in phase [$\Phi(\Psi)=180+180°$]. The phase-vector diagram for this case is shown in Fig. 3(*c*).

For triplet phases of Φ_Σ near $\pm90°$ the Ψ-scan profiles are nearly symmetrical, but there are significant differences. By means of the phase-vector diagrams Figs. 3(*b*) and (*d*) it is shown that for Φ_Σ near +90° there is a nearly symmetrical decrease, whereas for Φ_Σ near −90° an increase of the two-beam intensity results. This behaviour can also be deduced from (16). For $\Phi_\Sigma=+90°$ the interference term (cos

term) is always negative [$90 < \Phi(\Psi) < 270°$] and for $\Phi_\Sigma = -90°$ it is always positive [$-90 < \Phi(\Psi) < 90°$].

(*b*) *Calculated Ψ-scan profiles*

To confirm the results of the previous section we calculated Ψ-scan profiles on the basis of the exact dynamical theory for the three-beam case. The details of the calculations were reported recently (Hümmer & Billy, 1982).

As a non-centrosymmetric model structure we chose L-asparagine monohydrate ($C_4H_{10}N_2O_4$), space group $P2_12_12_1$ and lattice parameters $a = 5{\cdot}6$, $b = 9{\cdot}8$, $c = 11{\cdot}8$ Å; $Z = 4$. The structure factors were calculated on the basis of the enantiomorphic form of the published structure (Kartha & De Vries, 1961) (*i.e.* all the published atomic coordinates were taken with reversed sign). The structure factor moduli are given in Table 1. The triplet phases calculated from the known structure are indicated in Figs. 3 and 4.

For the calculations of the Ψ-scan profiles the following parameters were used: wavelength: Cu $K\alpha$, $\lambda = 1{\cdot}54$ Å; wavelength spread: $\Delta\lambda/\lambda = 3 \times 10^{-4}$; divergence of the primary beam: 2 min of arc; Ψ-scan sense: in-out; geometrical alignment: Bragg-Bragg* or Bragg-Laue.* The Ψ-scan rocking curves were calculated for the reflection $\mathbf{h} = 2\bar{1}2$ involved in various triplets with different triplet phases.

The results are shown in Fig. 3. The calculated profiles confirm the typical features of the Ψ-scan profiles for different triplet phases, which can be immediately deduced from the corresponding phase-vector diagram.

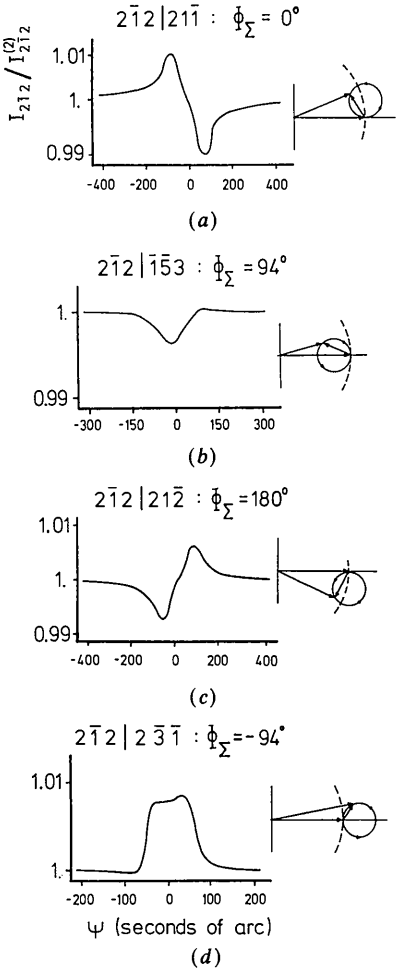

Fig. 3. Calculated Ψ-scan profiles for L-asparagine for four different triplet phases Φ_Σ and the corresponding phase-vector The integrated intensity $I_{(2\bar{1}2)}$ is normalized with respect to the two-beam level $I^{(2)}_{2\bar{1}2}$. The two sets of indices indicate the Bragg reflections due to **h** and **g**, which are in their diffraction positions at the three-beam setting. The triplet phase calculated from the known structure is given by $\Phi_\Sigma = \varphi(-\mathbf{h}) + \varphi(\mathbf{g}) + \varphi(\mathbf{h}-\mathbf{g})$.

5. Determination of enantiomorphs

For a non-centrosymmetric space group there are two enantiomorphic forms: the structure (S) with atomic coordinates $\mathbf{r}_j$ and the inverse (I) with atomic coordinates $\mathbf{r}'_j = -\mathbf{r}_j$. If the same origin is chosen for both forms the structure factors differ in the sign of their imaginary parts and their phases are related by $\Phi_S(\mathbf{h}) = -\Phi_I(\mathbf{h})$. Therefore, the triplet phase sums of S and I have opposite signs independent of the choice of the origin: $\Phi_\Sigma(S) = -\Phi_\Sigma(I)$ (Rogers, 1980). Hence, best selectors for S and I are triplet phases with $\Phi_\Sigma = \pm 90°$. Since both cases can be distinguished by means of the Ψ-scan profiles the absolute configuration can be fixed with only *one* measurement.

6. Discussion

As discussed above there are four typical Ψ-scan profiles for the triplet phases $\Phi_\Sigma = 0, \pm 90, 180°$. It should therefore be possible to determine experimentally at least the quadrant of the triplet phase involved in the three-beam diffraction by means of the measured profile, and at the same time the

* This notation is defined in Hümmer & Billy (1982).

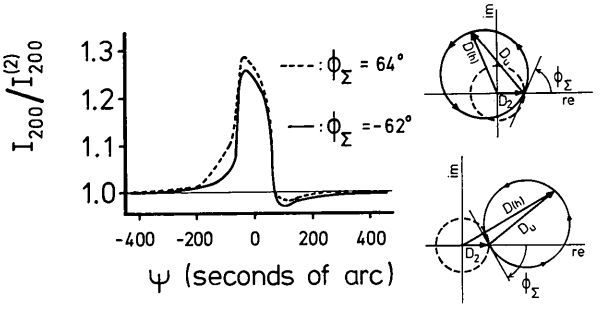

Fig. 4. Calculated Ψ-scan profiles for L-asparagine and the corresponding phase-vector diagrams for two different triplets in the case of a weak direct wave and a strong *Umweg* wave. 200/1$\bar{1}$3, $\Phi_\Sigma = -62°$: full line; 200/$\bar{1}\bar{1}$3, $\Phi_\Sigma = 64°$: dashed line; $|F(200)| = 16$; $|F(113)| = 81$.

Table 1. *Triplet phases and moduli of the structure factors for the calculated Ψ-scan profiles of Fig. 3*

Φ_Σ	**h**	**g**	$\lvert F(\mathbf{g})\rvert$	$\lvert F(\mathbf{h}-\mathbf{g})\rvert$
0°	$2\bar{1}2$	$21\bar{1}$	40	24
94°	$2\bar{1}2$	$\bar{1}\bar{5}3$	33	24
180°	$2\bar{1}2$	$21\bar{2}$	44	33
266°	$2\bar{1}2$	$23\bar{1}$	24	24

$|F(-\mathbf{h})| = |F(\bar{2}1\bar{2})| = 44$; $|F(\mathbf{O})| = 321$

absolute configuration can be fixed. But there are some basic requirements which have to be met in order to measure these typical Ψ-scan profiles in the experiment.

First of all, the maximum amplitudes of the interfering waves should be approximately of the same magnitude. Apart from the resonance terms R, the amplitudes are governed by the product of the structure factors F and the geometrical coupling factors α [*cf.* (10)]. In our theoretical and experimental results, the products $\alpha_n^m F(\mathbf{m}-\mathbf{n})$ should not differ from one another by a factor of two. This also implies that the α's must not equal zero. For instance, if α_g^h is approximately zero, then a strong wave may be propagated in the $K(\mathbf{g})$ direction but it cannot interact with the direct wave [*cf.* (10)]. That means that a second channel $K(\mathbf{g})$ is opened where energy can flow out and the two-beam intensity is always decreased in such a case. If the amplitude of the direct wave is too small then there will always result an increase of the two-beam intensity because of the relatively high amplitude of the *Umweg* wave. [*Umweg-Anregung* (Renninger, 1937)]. In such a case, shown in Fig. 4, there is no essential difference between the Ψ-scan profiles of different triplet phases, *i.e.* the phase information is lost. These facts can be seen from the phase-vector diagram in Fig. 4. On the other hand, if a strong direct wave interacts with a weak *Umweg* wave the dominant process will be scattering into the $K(\mathbf{g})$ direction *via* the r.l.v. $\mathbf{g}-\mathbf{h}$. Then the amplitude of the direct wave is diminished and a decrease in the two-beam intensity results. Calculations (Mayer, 1928) showed that this decrease is largely independent of the triplet phase (*Auffhellung*).

Secondly, the divergence and the spectral width of the primary beam must be small enough, since the ideal dynamical angular range of the three-beam interaction is $|\Psi| \simeq 10''$. As has already been discussed (Hümmer & Billy, 1982), the greater the divergence, the smaller is the change of the two-beam intensity level.

Thirdly, we have pointed out (Hümmer & Billy, 1982) that the absorption effects are not fundamental in explaining the asymmetry of the Ψ-scan profiles (Post, 1983), since for $\mu_0 t < 0{\cdot}5$ there is no significant difference with respect to the asymmetry for both diffraction geometries, transmission (Laue–Laue and Laue–Bragg) and reflection (Bragg–Laue and Bragg–Bragg) (μ_0: linear absorption coefficient; t: crystal thickness). However, for $\mu_0 t > 0{\cdot}5$, anomalous absorption effects may drastically change the typical profiles in the transmission case, while there is no essential influence on the reflection case. This means that the profiles become independent of the crystal shape for $\mu_0 t < 0{\cdot}5$, since for arbitrarily shaped crystals there is always a mixture of both diffraction geometries.

In conclusion, we are aware of the fact that the outlined simple phase-vector diagram for the interference of the direct and the *Umweg* wave cannot explain all the details of the Ψ-scan profiles. It is not valid very close to the three-beam position because the denominator N of (11) is no longer a constant. In this range $R(\mathbf{g})$ may rise to 10^6, and all the resonance terms $R(\boldsymbol{n})$ depend on the intersection of the dispersion surfaces, which depends on the diffraction geometry. These effects are all included in the calculations based on the dynamical theory. They may play an important role in discussing the details of the Ψ-scan profiles in the case of a very weak direct reflection, for instance Ge(222), as was done by Juretschke (1984). We know from our theoretical calculations that there is a tendency to increase the two-beam intensity in the Bragg case, whereas in the Laue case an overall decrease of the intensity is observed. This can also be seen by comparing Figs. 3(*b*) and (*d*). Since there is a mixture of both geometries for an arbitrarily shaped crystal, these opposite tendencies may compensate each other in the real experiment.

However, by means of the phase-vector diagram the general features of the Ψ-scan profiles can be deduced even in the case of non-centrosymmetric structures and it throws light upon the physics of the three-beam interference.

Experimental results concerning the determination of triplet phases of asparagine monohydrate will be reported in a second paper. We have already reported the main results at ECM8 in Liège (Hümmer & Billy, 1983) and the XIIIth Congress of the IUCr in Hamburg (Hümmer & Billy, 1984; Billy, Burzlaff & Hümmer, 1984)

We gratefully acknowledge helpful discussions with Professor Dr H. Burzlaff.

References

BETHE, H. A. (1928). *Ann. Phys. (Leipzig)*, **87**, 55-129.
BILLY, H., BURZLAFF, H. & HÜMMER, K. (1984). *Acta Cryst.* A**40**, C409.
CHANG, S. L. (1982). *Phys. Rev. Lett.* **48**, 163-166.
EWALD, P. P. (1917). *Ann. Phys. (Leipzig)*, **54**, 519-597.
EWALD, P. P. (1965). *Rev. Mod. Phys.* **37**, 46-56.
EWALD, P. P. & HÉNO, Y. (1968). *Acta Cryst.* A**24**, 5-15.
HØIER, R. & MARTHINSEN, K. (1983). *Acta Cryst.* A**39**, 854-860.
HÜMMER, K. & BILLY, H. (1982). *Acta Cryst.* A**38**, 841-848.

HÜMMER, K. & BILLY, H. (1983). *Eighth European Crystallographic Meeting, Liège. Abstracts*, p. 252.
HÜMMER, K. & BILLY, H. (1984). *Acta Cryst.* A**40**, C348.
JURETSCHKE, H. J. (1982*a*). *Phys. Rev. Lett.* **48**, 1487–1489.
JURETSCHKE, H. J. (1982*b*). *Phys. Lett. A*, **92**, 183–185.
JURETSCHKE, H. J. (1984). *Acta Cryst.* A**40**, 379–389.
KARTHA, G. & DE VRIES, A. (1961). *Nature (London)*, **192**, 862–863.
LAUE, M. VON (1960). *Röntgenstrahlinterferenzen.* Frankfurt (Main): Akademische Verlagsgesellschaft.
LIPSCOMB, W. N. (1949). *Acta Cryst.* **2**, 193–194.
MAYER, G. (1928). *Z. Kristallogr.* **66**, 585–636.
POST, B. (1983). *Acta Cryst.* A**39**, 711–718.
RENNINGER, M. (1937). *Z. Phys.* **106**, 141–176.
ROGERS, D. (1980). *Theory and Practice of Direct Methods in Crystallography*, edited by M. F. C. LADD & R. A. PALMER. New York: Plenum Press.

SHORT COMMUNICATIONS

Contributions intended for publication under this heading should be expressly so marked; they should not exceed about 1000 *words; they should be forwarded in the usual way to the appropriate Co-editor; they will be published as speedily as possible.*

Acta Cryst. (1986). A**42**, 133–134

Note on 3D (3, 4)-connected nets.

By A. F. WELLS, *Department of Chemistry and Institute of Materials Science, The University of Connecticut, Storrs, CT* 06268, *USA*

(*Received* 2 *July* 1985; *accepted* 9 *September* 1985)

Abstract

Three new 3D (3, 4)-connected nets are described belonging to the special family of nets in which each 3-connected point is connected to three 4-connected points and each 4-connected point is connected to four 3-connected points.

In earlier accounts of three-dimensional nets (Wells, 1977, 1979) it was noted that a special family of 3D (3, 4)-connected nets comprises those in which every 3-connected point is connected to three 4-connected points and every 4-connected point to four 3-connected points. These nets represent actual or possible structures of compounds A_3X_4 in which A and X are the 4- and 3-connected atoms respectively. Since the unit cell in an ordered structure must contain one or more A_3X_4 the total number Z' of 3- and 4-connected atoms must be a multiple of 7, that is, $Z'=7Z$ for a unit cell containing $Z(A_3X_4)$. The only nets of the $Z'=7m$ family that were described previously were one cubic net with $Z'=7$ and two nets with $Z'=14$. A by-product of a survey of tetrahedral structures (Wells, in preparation) was the recognition of three more nets of the $Z'=7m$ family, all with $Z'=14$. These are the nets 2, 3 and 4 listed below. The structures based on net 3 have been known for some time, but were not described as examples of a net of this type.

Accordingly we may now list six nets of the $Z'=7m$ family. The first five can be built with regular tetrahedral coordination of the 4-connected A atoms and are illustrated as structures built from regular tetrahedra in the survey referred to above. In the most symmetrical configuration of the sixth net there is square coplanar coordination of the 4-connected points. The coordination of the 3-connected points is exactly or approximately trigonal coplanar in nets 6 and 5 respectively but pyramidal in nets 1–4. The two cubic nets 1 and 6 are the only two of this family in which all 3-connected points are symmetrically equivalent and all 4-connected points are symmetrically equivalent. The detailed descriptions of the most symmetrical configurations of the nets are as follows:

1. $(6^3)_4(6^28^4)_3$ Space group $P\bar{4}3m$ (No. 215) $Z'=7$

$$v_3\ 4(e)\ (xxx)\ x=\tfrac{1}{4}$$
$$v_4\ 3(d)\ (\tfrac{1}{2}00)$$

2. $(6^3)_6(8^3)_2(6^38^3)_6-a$ Space group $P6_3mc$ (No. 186) $Z'=14$

$$v_3\begin{cases}2(b)\ (\tfrac{1}{3}\tfrac{2}{3}z)\ z=\tfrac{1}{2}\\ 6(c)\ (x\bar{x}z)\ x=\tfrac{1}{6}\ z=0\end{cases}$$
$$v_4\ 6(c)\ (x\bar{x}z)\ x=\tfrac{1}{6}\ z=\tfrac{3}{8}$$
$$c:a=\sqrt{2}/\sqrt{3}$$

3. $(6^3)_8(6^38^3)_2(6^28^4)_4$ Space group $I\bar{4}2m$ (No. 121) $Z'=14$

$$v_3\ 8(i)\ (xxz)\ x=\tfrac{1}{4}\ z=\tfrac{3}{8}$$
$$v_4\begin{cases}2(a)\ (000)\\ 4(d)\ (0\tfrac{1}{2}\tfrac{1}{4})\end{cases}$$
$$c:a=2$$

4. $(6^3)_2(6.8^2)_2(6^3)_4(6^38^3)_2(6^48^2)_4$ Space group $Pmn2_1$ (No. 31) $Z'=14$

$$v_3\begin{cases}2(a)\ (0yz)\ y=\tfrac{1}{3}\ z=\tfrac{15}{16}\\ 2(a)\ (0yz)\ y=\tfrac{2}{3}\ z=\tfrac{7}{16}\\ 4(b)\ (xyz)\ x=\tfrac{1}{4}\ y=\tfrac{1}{6}\ z=\tfrac{7}{16}\end{cases}$$
$$v_4\begin{cases}2(a)\ (0yz)\ y=\tfrac{1}{3}\ z=\tfrac{9}{16}\\ 4(b)\ (xyz)\ x=\tfrac{1}{4}\ y=\tfrac{1}{6}\ z=\tfrac{1}{16}\end{cases}$$
$$a:b:c=2/\sqrt{3}:1:2\sqrt{2}/3$$